



# CryoEM and Molecular Dynamics of the Circadian KaiB–KaiC Complex Indicates That KaiB Monomers Interact with KaiC and Block ATP Binding Clefts

Seth A. Villarreal<sup>1</sup>, Rekha Pattanayek<sup>2</sup>, Dewight R. Williams<sup>3</sup>, Tetsuya Mori<sup>4</sup>, Ximing Qin<sup>4</sup>, Carl H. Johnson<sup>4</sup>, Martin Egli<sup>2</sup> and Phoebe L. Stewart<sup>1</sup>

**1 - Department of Pharmacology and Cleveland Center for Membrane and Structural Biology, Case Western Reserve University, Cleveland, OH 44106, USA**

**2 - Department of Biochemistry, Vanderbilt University, School of Medicine, Nashville, TN 37232, USA**

**3 - Department of Molecular Physiology and Biophysics, Vanderbilt University, School of Medicine, Nashville, TN 37232, USA**

**4 - Department of Biological Sciences, Vanderbilt University, Nashville, TN 37235, USA**

**Correspondence to Phoebe L. Stewart:** [phoebe.stewart@case.edu](mailto:phoebe.stewart@case.edu)

<http://dx.doi.org/10.1016/j.jmb.2013.06.018>

**Edited by J. Johnson**

## Abstract

The circadian control of cellular processes in cyanobacteria is regulated by a posttranslational oscillator formed by three Kai proteins. During the oscillator cycle, KaiA serves to promote autophosphorylation of KaiC while KaiB counteracts this effect. Here, we present a crystallographic structure of the wild-type *Synechococcus elongatus* KaiB and a cryo-electron microscopy (cryoEM) structure of a KaiBC complex. The crystal structure shows the expected dimer core structure and significant conformational variations of the KaiB C-terminal region, which is functionally important in maintaining rhythmicity. The KaiBC sample was formed with a C-terminally truncated form of KaiC, KaiC-Δ489, which is persistently phosphorylated. The KaiB–KaiC-Δ489 structure reveals that the KaiC hexamer can bind six monomers of KaiB, which form a continuous ring of density in the KaiBC complex. We performed cryoEM-guided molecular dynamics flexible fitting simulations with crystal structures of KaiB and KaiC to probe the KaiBC protein–protein interface. This analysis indicated a favorable binding mode for the KaiB monomer on the CII end of KaiC, involving two adjacent KaiC subunits and spanning an ATP binding cleft. A KaiC mutation, R468C, which has been shown to affect the affinity of KaiB for KaiC and lengthen the period in a bioluminescence rhythm assay, is found within the middle of the predicted KaiBC interface. The proposed KaiB binding mode blocks access to the ATP binding cleft in the CII ring of KaiC, which provides insight into how KaiB might influence the phosphorylation status of KaiC.

© 2013 Elsevier Ltd. All rights reserved.

## Introduction

The cyanobacterial clock is an elegant nanomachine that maintains remarkable synchronicity despite cell division and temperature fluctuations and can be entrained by light/dark cycles possibly involving light-driven changes in energy metabolism [1,2]. *Synechococcus elongatus* contains one of the simplest clocks in which three proteins, KaiA, KaiB, and KaiC in the presence of ATP, form a posttranslational oscillator (PTO) [3]. *In vitro*, this clock ticks through daily cycles of KaiC phosphorylation and dephosphorylation for up to 10 days in

the absence of a translation–transcription feedback loop [4]. This clock is temperature compensated [3,5], which minimizes the role of daily environmental fluctuations, remains accurate during cell divisions, and has a built-in ratcheting mechanism to ensure that the *in vitro* KaiABC reaction is unidirectional [6,7].

Study of this system, including crystal structures of individual proteins and evaluation of protein–protein interactions, has revealed salient features of the PTO and its relationship to a translation–transcription feedback loop for modulation of transcriptional oscillation of clock-regulated genes [6]. During the

course of a single PTO cycle, there is a strict order of phosphorylation and dephosphorylation of KaiC. KaiA promotes KaiC phosphorylation first at T432 and subsequently at S431 [8,9]. KaiB is then recruited to the KaiA–KaiC complex, which sequesters KaiA, and allows the circadian cycle to proceed [9–12]. KaiC dephosphorylates, at least partially via ADP phosphotransferase activity [13,14], pT432 first followed by pS431, which returns KaiC to the initial state of the cycle [3]. Throughout the oscillation cycle, KaiC exists as a population differentiated by the ratios of various states (monomeric and hexameric KaiC, KaiAC, KaiBC, and KaiABC). Synchronicity is maintained in part by subunit exchange of the KaiC hexamer with the free monomers within the cell [15,16] and by KaiA sequestration [9,12,17]. *In vivo*, the histidine kinase SasA relays the phosphorylation state of the PTO to transcription factors, including RpaA and RpaB, to influence global transcription rhythms [18–20].

The *S. elongatus* KaiC crystal structures of wild type, mutants, and phospho-mimics reveal a hexamer, forming a “double-doughnut” of stacked N-terminal CI and C-terminal CII rings (KaiCI and KaiCII) with a central channel, and two main phosphorylation sites, S431 and T432, at the subunit interface [21,22]. Despite a high degree of homology between the two KaiC domains, they appear to have distinct functions. The CI domain may act as an input-independent timer and the CII domain may sense the ATP/ADP ratio in the cell [23]. The KaiC hexamer binds 12 ATP molecules, one between each subunit interface in both the CI and CII rings [24]. The *S. elongatus* KaiA crystal structure shows a dimer with a domain-swapped arrangement [25]. KaiA binds the KaiCII ring via the KaiC C-terminal tails and stimulates KaiC autokinase activity [22,26–28]. KaiB interacts with the phosphorylated form of KaiC and facilitates the return of KaiC to the unphosphorylated state [29]. In crystals and in solution, KaiB forms a tetramer [30–33]. The component protein structures provide a good starting point for biophysical characterization of the assemblies formed by this nanomachine during the PTO cycle.

The KaiBC complex has been studied by electron microscopy (EM) [33], small-angle X-ray scattering (SAXS) [11,34], and most recently by EM with gold labeling of KaiC in complex with KaiB [35]. In the first SAXS study, a tetrameric state of KaiB was assumed from the existing crystal structures [34]. In contrast, the first EM study of KaiBC clearly showed a third layer of density above the KaiC hexamer and with a shape appropriate for two KaiB dimers [33]. The finding that KaiB binds KaiC as a dimer was unexpected because all KaiB crystal structures show a tetrameric state [30–33]. A more recent SAXS study of KaiB alone and in complex with KaiC confirmed a tetrameric state for KaiB in

solution and a dimeric state in the KaiBC complex [11]. Modeling of this KaiBC SAXS envelope with a pair of KaiB dimers, a single tetramer, or a pair of tetramers indicated a best match with two KaiB dimers bound to the KaiC hexamer, consistent with the EM-based model [33].

The similarity of the two ends of the KaiC hexamer, the CI and CII rings, has made the question of where KaiB binds on the KaiC hexamer difficult to answer and has led to a continuing debate. In the Akiyama *et al.* SAXS study, it was supposed that KaiB binds to the CII ring of KaiC on the basis of the KaiC C-terminal tails, which were assigned within the low-resolution SAXS envelope on the same side of the complex as KaiB [34]. A few months later, a native PAGE assay of the individually expressed *S. elongatus* KaiC CI and CII domains indicated that *S. elongatus* KaiB binds CII but not CI [33]. In a more recent SAXS study by Pattanayek *et al.*, the envelope for KaiC in solution showed the KaiC C-terminal tails protruding from the CII side of the hexamer [11]. In the KaiBC SAXS envelope of the same study, the KaiC C-terminal tails were docked between two KaiB dimers modeled on the CII side of the hexamer to produce a model that agreed with the SAXS envelope. The question of where the KaiB binding site is located on the KaiC hexamer was revisited by Chang *et al.* with gel-filtration chromatography and NMR binding experiments [36]. Their results indicated that a mutated form of *Thermosynechococcus elongatus* KaiB, which preferentially assembles as dimers in solution, formed detectable complexes with an individually expressed form of the KaiC CI domain, but not with the individually expressed KaiC CII (S431 mutant) domain. These results led them to propose that KaiB must bind to the CI ring of the intact KaiC hexamer. Phong *et al.* have shown that KaiC with two catalytic mutations in the CI ring, E77Q and E78Q, does not bind KaiB [23]. The location of these mutations is within the middle of the CI ring, rather than on the surface of KaiC, suggesting that their effect must be transferred to the KaiB binding site on KaiC. Most recently, EM studies of KaiB in complex with KaiC S431D mutant hexamers with C-terminal His6 tags labeled with nickel(II) nitrilotriacetic acid gold nanoparticles (Ni-NTA-Nanogold) showed that the dense gold particles are located on the same side as KaiB [35]. This work provides direct evidence for KaiB binding on the CII ring of the KaiC hexamer, which places KaiB close to the main KaiC phosphorylation sites, and near the KaiA binding site on the KaiC C-terminal tails.

Critical interactions between two loops of a KaiC subunit are disrupted upon KaiA binding [26]. This local disruption is propagated to neighboring KaiC subunits, leading to enhanced flexibility within the

KaiC CII ring and increased phosphorylation of KaiC. The action of KaiA in promoting KaiC phosphorylation is opposed by KaiB and may involve sequestration of KaiA in a ternary KaiABC complex, in which KaiA has an alternative binding mode to KaiC or KaiBC [11]. The molecular mechanisms underlying the action of KaiB on KaiC and the KaiABC complex are poorly understood. Knowledge of the protein–protein interface between KaiB and KaiC would help elucidate the molecular mechanisms underlying the action of KaiB during the PTO cycle. We present a crystal structure of wild-type *S. elongatus* KaiB and a cryo-electron microscopy (cryoEM) structure of a KaiBC complex. We used molecular dynamics flexible fitting (MDFF) simulations to examine the protein–protein interface of KaiB relative to KaiC. We propose that six KaiB monomers interact with a KaiC hexamer at the KaiCII side and effectively block the ATP binding clefts on KaiCII.

## Results

### Crystal structure of *S. elongatus* KaiB

Crystal structures of the KaiB proteins from the cyanobacteria *Anabaena* [30], *Synechocystis* [31], and *T. elongatus* (T64C mutant [32] and wild type [33]) were previously determined. In all cases, the protein forms a dimer of dimers with the core (amino acids Y7–Y93; *S. elongatus* KaiB numbering) of monomeric subunits and the tetramer adopting very similar conformations in all four structures, consistent with highly conserved sequences across species in that region (Fig. S1). Crystals of *S. elongatus* KaiB were grown from mixtures of the KaiB and KaiC proteins, and the structure was determined by molecular replacement at a resolution of 2.6 Å. The asymmetric unit in space group *C2* reveals a single tetramer (Fig. S2) and, except for six N-terminal residues from subunit a, all 102 residues for subunits a to d could be built into the electron density. Examples of the quality of the final electron density are depicted in Fig. 1a and b, and selected data collection and refinement parameters are summarized in Table 1.

The KaiB dimer resembles a trapezoid with a base dimension of ca 60 Å, a height of 30 Å, and a thickness (Y7–Y93 core) of ca 30 Å (Fig. S2a). However, N- and C-terminal tails from subunits a/c and b/d (a/b, dimer 1, and c/d, dimer 2) jut out on opposite sides of the more or less flat KaiB tetramer, thus approximately doubling the thickness of the assembly (Fig. S2b). Within the monomer, residues Y7 and Y93 stitch together two β-strands six and eight residues from the N- and C-termini, respectively. These tyrosines also play a key role in the

stabilization of the dimer–dimer interface, where they form mostly hydrophobic contacts (Fig. S3). Their importance in the formation of the dimer of dimers is supported by the fact that the KaiB Y7,93A double mutant was found to exist predominantly in the dimeric form [36]. N- and C-terminal tails extend in a wishbone-like arrangement from the Y7–Y93 core structure (Fig. 1c and d; Fig. S2b), and no direct association between the first six and the last eight residues appears to exist in the 102-residue monomeric subunits. While core residues are highly conserved in KaiB proteins from diverse cyanobacteria, the lengths and sequences of the C-terminal region vary widely (Fig. S1). Clustered acidic residues represent a common feature, and Iwase *et al.* previously demonstrated that glutamates and aspartates in the KaiB C-terminal tail play a critical role in maintaining rhythmicity [32]. However, without high-resolution structures of the binary KaiB–KaiC and/or the ternary KaiA–KaiB–KaiC complex, it has remained unclear how KaiB C-terminal residues influence clock period and amplitude. Thus, it is possible that the tail simply affects the dimer–tetramer equilibrium [37], whereby only dimers interact with KaiC. Alternatively, the KaiB C-terminal region could somehow affect the course of KaiC dephosphorylation by interfering with the KaiC active site at subunit interfaces or serve to enhance the interaction between the KaiB–KaiC complex and KaiA near the end of the daily clock cycle [11]. A superimposition of monomeric subunits from the *S. elongatus* KaiB crystal structure illustrates significant conformational variations of the C-terminal region (Fig. S4).

### CryoEM structure of the KaiB–KaiC complex formed with KaiC-Δ489

KaiB forms a complex with KaiC hexamers following autophosphorylation of KaiC at serine 431 [8,38]. During circadian oscillation, this site is transiently phosphorylated, and less than 30% of the KaiC hexamers are in complex with KaiB [16]. To enrich for the KaiB–KaiC (KaiBC) complex for cryoEM structure determination, we investigated complexes assembled with three mutant forms of KaiC. Two mutants, KaiC-S431E-T432E and KaiC-S431D, are phosphomimetic mutants while the third, KaiC-Δ489, is a truncation mutant lacking 30 amino acids from the C-terminus. This C-terminal truncation results in a mutant form of KaiC that is hyperphosphorylated [27] and forms a stable complex with KaiB [12]. Micrographs of a negatively stained KaiBC sample formed with KaiC-S431E-T432E showed a high background level of a protein about the size of a KaiC subunit. This suggested that the KaiC-S431E-T432E hexamer might not be stable in the presence of KaiB. Native-PAGE analysis of this sample confirmed that approximately 10–30% of KaiC is in the

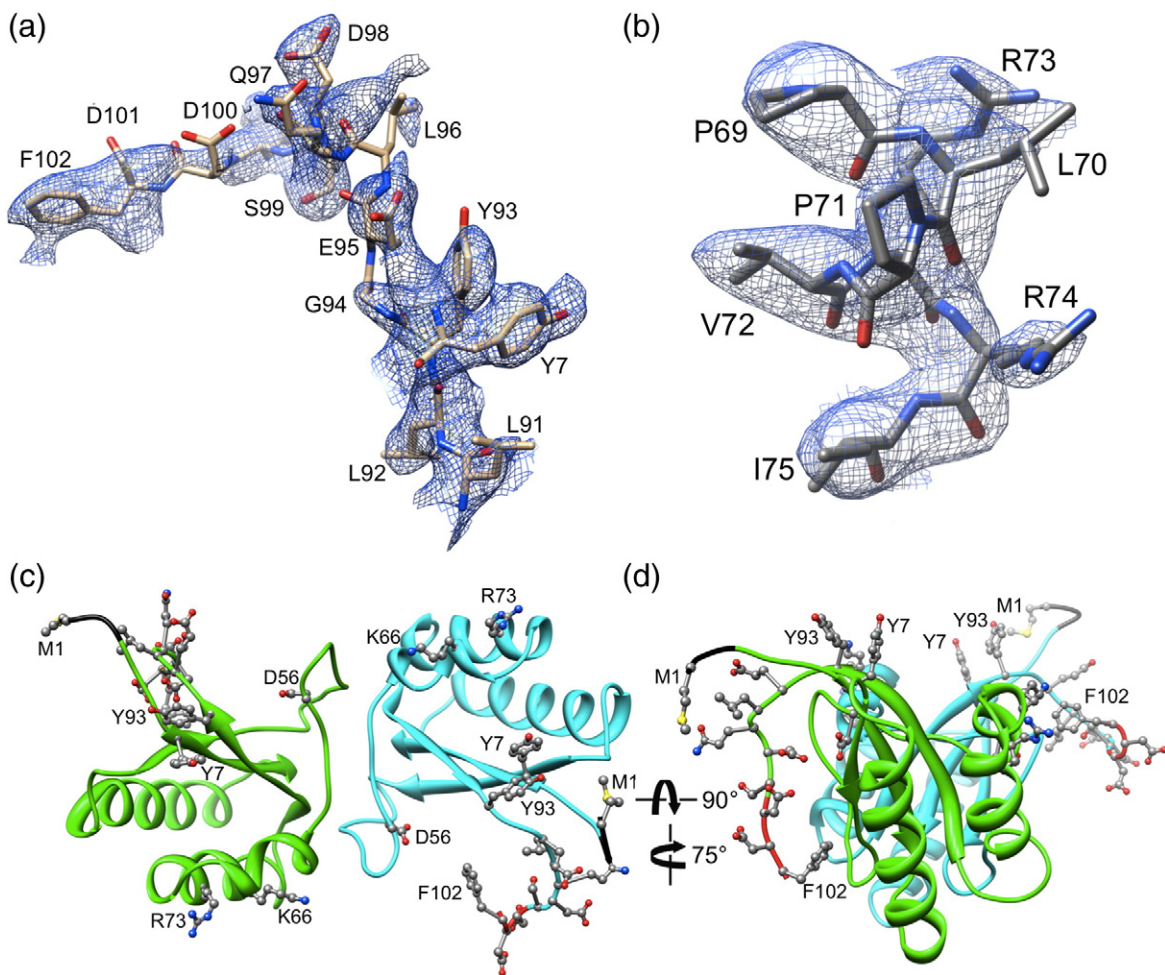


**Fig. 1.** Crystal structure of *S. elongatus* KaiB. Quality of the final electron density (a) in the region of the C-terminal tail of subunit a and (b) around residues P69 to I75 of subunit c. The Fourier  $2F_o - F_c$  sum electron density map is drawn at the  $1 \sigma$  level. The KaiB dimer (c, green, and d, cyan, subunits) viewed (c) approximately along the non-crystallographic dyad and (d) rotated around the horizontal and the vertical to illustrate the wishbone-like arrangement of N- and C-terminal tails. N- and C-terminal portions of the ribbon are highlighted in black and red, respectively, with side chains of selected residues depicted in ball-and-stick mode.

monomeric form [12]. Cryo-electron micrographs of the KaiBC sample formed with the second form of KaiC, KaiC-S431D, displayed a preferred orientation for the complex with the predominant view along the 6-fold axis of the KaiC hexamer (top view). Cryo-electron micrographs of the KaiBC sample formed with the third form of KaiC, KaiC- $\Delta$ 489, displayed the best properties for a cryoEM structural analysis, with reasonably uniform and well-dispersed particles. Therefore, we collected a cryoEM data set of this third complex with a total of 195,226 particle images.

In order to select subsets of particle images with high KaiB occupancy, we performed an Eigen-image analysis similar to that performed for GroEL by Clare *et al.* [39]. This led to the selection of side-view particles and further sorting of the side-view particle images with high KaiB occupancy

(~60%) or low KaiB occupancy (~40%). Reference free image classification was performed on both subsets followed by three-dimensional structure calculation without imposed symmetry using a 30-Å filtered representation of the KaiC crystal structure (amino acids 14–489) as the starting model. The high KaiB occupancy subset resulted in a class-average-based structure with a third layer of KaiB density, whereas the low KaiB occupancy subset resulted in a structure resembling KaiC without the third layer of density (Fig. S5). Projections of the high KaiB occupancy class-average-based structure resemble the matching class averages of this subset (Fig. 2a). During refinement of the particle images in the high KaiB occupancy subset, it became apparent that the KaiBC structure displayed approximate 6-fold symmetry for both the KaiB and KaiC density layers, and

**Table 1.** KaiB crystal structure statistics

<i>Data collection</i>	
Space group	C2
Cell dimensions: <i>a</i> , <i>b</i> , <i>c</i> (Å), $\beta$ (°)	69.82, 116.12, 53.23, 98.3
Wavelength (Å)	0.98
Resolution (Å) (last shell)	30.00–2.60 (2.69–2.60)
Unique reflections (last shell)	12,670 (1278)
Completeness (%) (last shell)	100.0 (99.9)
$R_{\text{merge}}$ (last shell)	0.060 (0.267)
$I/\sigma(I)$ (last shell)	14.6 (2.1)
<i>Refinement</i>	
Working set reflections	8966 [ $F \geq 3\sigma(F)$ ]
Test set reflections	423 (4.7%)
Protein atoms	3173
Solvent atoms	99
$R_{\text{work}}/R_{\text{free}}$	0.25/0.30
Average <i>B</i> -factors (Å <sup>2</sup> )	
Protein (all atoms)	78
Solvent	64
r.m.s.d.	
Bond lengths (Å)	0.003
Bond angles (°)	0.8
Ramachandran analysis (%)	
Most favored	81.9
Allowed	13.2

therefore C6 symmetry was imposed for the remaining refinement rounds. The best structure generated from the high KaiB occupancy subset was used as a search model for one round of systematic parameter search against the full data set (including top, side, and tilted views). We reasoned that since 60% of the side-view particle images were sorted with the high KaiB occupancy subset, probably ~60% of the full data set also had high KaiB occupancy. Therefore, we selected ~50% of the total data set, those particles with the highest cross-correlation values with the search model, to produce a final C6 symmetrized structure with a resolution of 16 Å at the Fourier shell correlation (FSC) 0.5 threshold (13 Å at the FSC 0.143 threshold) (Fig. 2b).

Overall, the cryoEM structure of KaiB–KaiC-Δ489 resembles the negative-stain EM KaiBC structure [33] but with a more complete ring of density assigned to KaiB. Presumably the negative-stain structure represents an average of particle images with various levels of KaiB occupancy, and the Eigenimage analysis of the cryoEM data set served to select a more uniform subset of particle images. The previous negative-stain EM KaiBC structure formed with wild-type KaiC did not show the flexible C-terminal tails of KaiC, which protrude from the CII end of KaiC, probably because of a high degree of conformational flexibility. Both the negative-stain EM and cryoEM structures display a double-doughnut shape recognizable as KaiC. The strong similarities between the two structures provide confidence that the truncation of KaiC did not adversely affect the binding location of KaiB or the overall conformation of the KaiBC complex. Both structures show a third layer of density assigned to KaiB; however, the

cryoEM structure shows KaiB density of the appropriate size for a KaiB monomer above each KaiC subunit (Fig. 2b).

### Docking of KaiB and KaiC crystal structures into the KaiB–KaiC-Δ489 density

To gain insight into the structural basis for how KaiB might influence the phosphorylation status of KaiC as well as promote the release of KaiA from a KaiABC complex, we built molecular models for the KaiBC complex. Given the nearly symmetrical shape of the KaiC hexamer and the absence of helical density rods within the cryoEM structure, it was not possible to determine from the cryoEM structure alone whether KaiB binds to the N-terminal CI or C-terminal CII end of the hexamer. However, we noted that the strongest cryoEM density within KaiC was farthest from the third layer of KaiB density, which would be consistent with the  $\alpha$ -helices of the CI domain at this position (Fig. S6). We have previously presented indirect evidence that KaiB binds to the CII ring of KaiC [33]. A recent negative-stain EM study, using KaiB and gold-labeled full-length KaiC, indicates that KaiB binds KaiCII [35]. Nevertheless, given the difficulty in distinguishing the two ends of KaiB by cryoEM, we built models for the KaiBC complex with KaiB interacting with either the CI or the CII end of KaiC.

An atomic model for KaiC-Δ489 was made by computationally removing 30 C-terminal residues from the KaiC crystal structure [Protein Data Bank (PDB) ID: 3DVL, amino acids 14–489]. In the crystal structure, four copies of Ser431 and all six copies of Thr432 are phosphorylated. These phosphorylated residues were retained, and the remaining two copies of Ser431 were computationally modified to the phosphorylated state with VMD 1.9 [40]. A fully phosphorylated form of KaiC was built because KaiB associates with phosphorylated KaiC more strongly than with non-phosphorylated KaiC [41,42]. In addition, a KaiC double phospho-mimic, S431D-T432D, has been shown to be more favorable for KaiBC complex formation than a KaiC mutant that mimics the unphosphorylated state, KaiC-S431A-T432A [37].

Two molecular models for KaiC-Δ489 were refined into the cryoEM density map using cryoEM-guided molecular-dynamics-based flexible fitting with MDFF and NAMD [43,44]. Both possible orientations of KaiC were tested, with the KaiC CI ring next to KaiB and the KaiC CII ring next to KaiB. Similar potential energies were obtained after MDFF simulations with KaiC docked in either orientation in the absence of KaiB. During MDFF, a standard potential energy function preserves correct stereochemistry, while application of an additional guiding force based on the cryoEM density map steers the coordinates into better

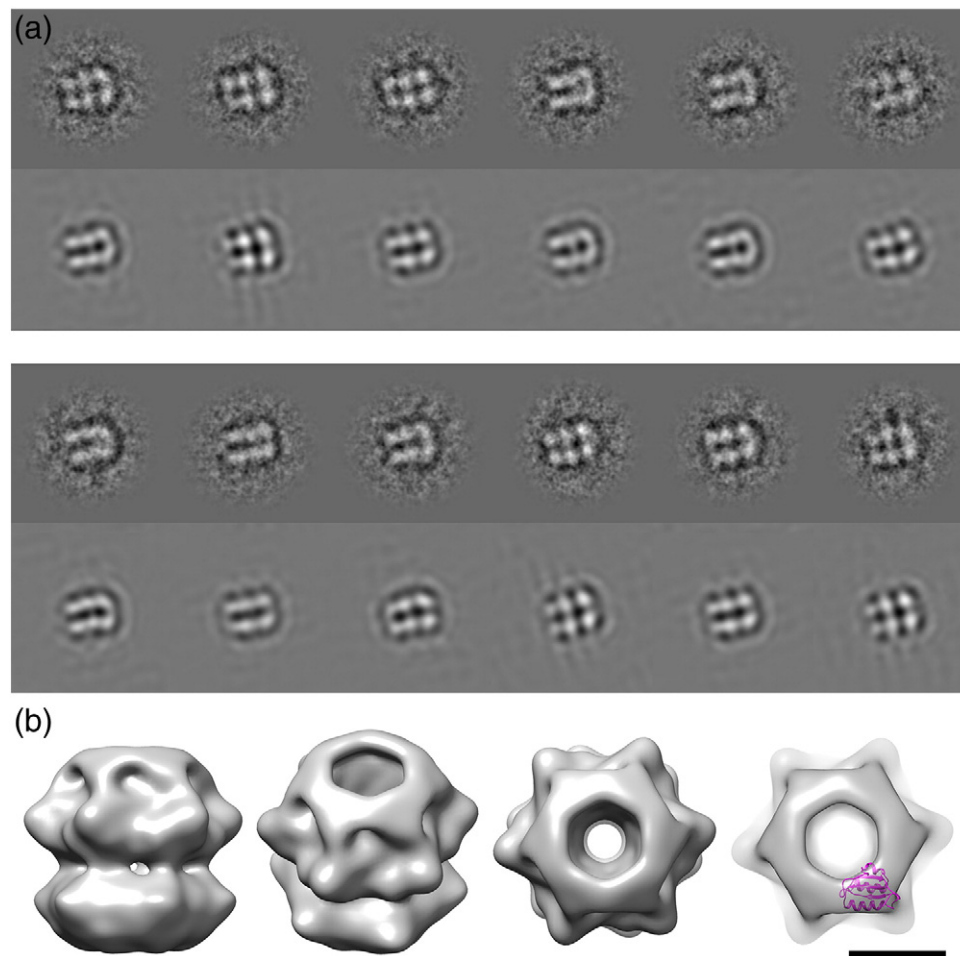


**Fig. 2.** CryoEM structure of KaiB–KaiC- $\Delta$ 489. (a) Selected cryoEM class averages and matching projections. The projected structure is a class-average-based structure generated from selected side-view particles with high KaiB occupancy at 29 Å resolution. (b) Final C6-symmetrized particle-image-based cryoEM structure at 16 Å resolution shown in side, 45° tilted, and top views. The rightmost panel shows a KaiB monomer (magenta) docked within the third layer of density. The scale bar represents 50 Å.

agreement with the density. This hybrid cryoEM/MDFF approach has been applied to several macromolecular complexes [45]. In the case of a cryoEM structure of human adenovirus in complex with coagulation factor X, an MDFF analysis led to identification of key residues at the interface, and one of these residues was confirmed by mutagenesis to be critical for the interaction [46].

For the KaiB monomer, we generated an atomic model lacking the C-terminal tail (cut after Y93) since the crystal structure of wild-type *S. elongatus* KaiB indicates that the tails are flexible (Fig. S4). Also Murakami *et al.* have shown that truncation of the C-terminal tails of *T. elongatus* KaiB, which has 89% identity with *S. elongatus* KaiB, increases the binding affinity of KaiB for a hyperphosphorylated mimic of KaiC by a factor of 15 [37]. The KaiB monomer was manually docked into the third layer of cryoEM density with USCF Chimera [47]. The

visually best fitting model (Fig. 2b) positioned the two longest  $\alpha$ -helices of KaiB against KaiC. Eight reasonably well-fitting positions for KaiB were generated: four with the  $\alpha$ -helices of KaiB against KaiC and rotated 90° with respect to each other, and four with the  $\beta$ -strand side of KaiB against KaiC and rotated 90° with respect to each other. All of the KaiB models were raised ~5 Å above the KaiC surface before the MDFF simulations.

All eight positions of KaiB were tested with the two orientations for KaiC, with the CI or CII side interacting with KaiB, in 100-ps MDFF simulations. The nonbonded interaction energies between a KaiB monomer and the KaiC hexamer at the ends of the simulations are reported in Table S1 for all of the models. Within the set of eight models that have KaiB interacting with KaiCII, there is one most favorable orientation for KaiB (model 1), which has a nonbonded interaction energy of  $-365$  kcal/mol

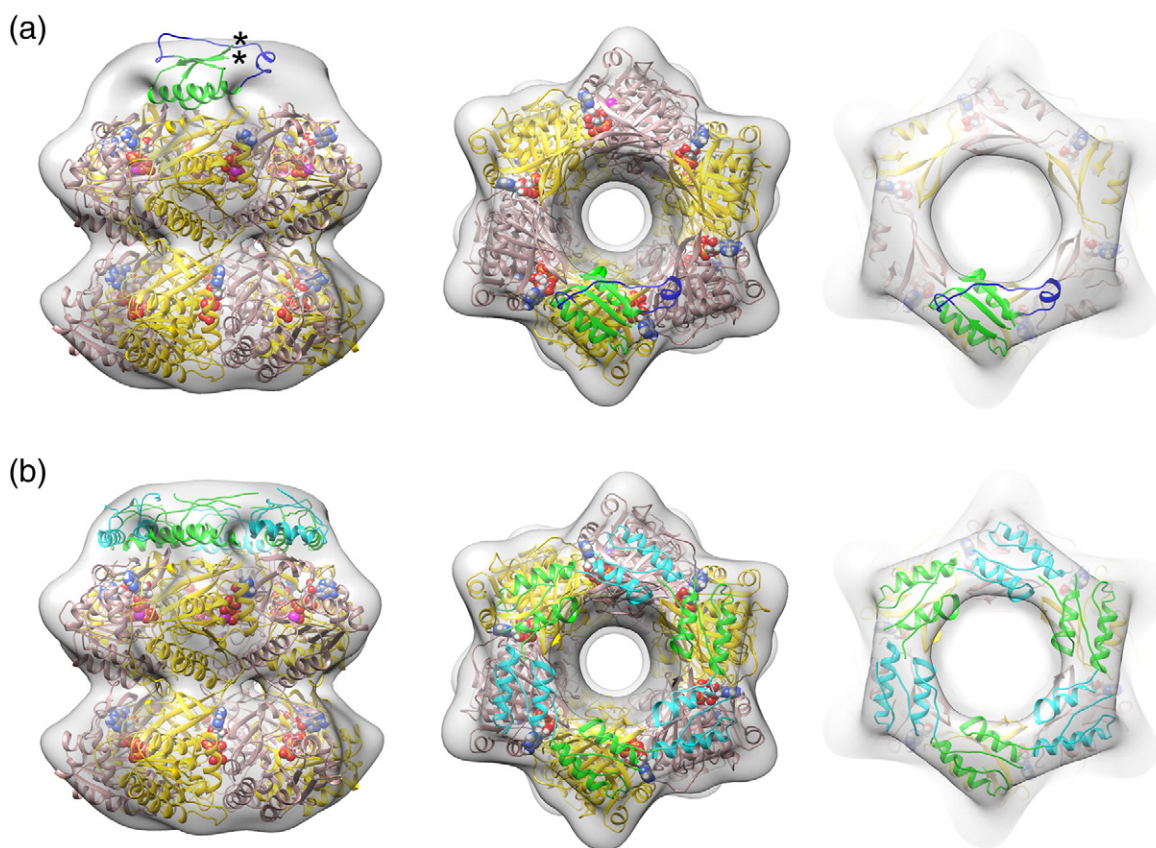


**Fig. 3.** KaiBC atomic model docked within the cryoEM density. (a) The best MDFF-refined model within the KaiBC cryoEM density (transparent gray). A KaiC hexamer (gold and brown ribbons) is shown with one KaiB monomer (green ribbon). The KaiB dimerization loop and short  $\alpha$ -helix (amino acids 45–69) are shown in blue. The asterisks mark the positions of the N- and C-terminal tails of KaiB missing from the docked core model of KaiB (amino acids 7–93). Twelve ATP molecules and 6  $Mg^{2+}$  are shown in space-filling representation and colored by element. (b) An MDFF-refined model with six KaiB monomers (green and cyan) forming a ring on the CII side of KaiC. The KaiB dimerization loops and short  $\alpha$ -helices were removed to limit steric clashes before the MDFF simulation with all six KaiB monomers.

and a buried accessible surface area between a KaiB monomer and a KaiC hexamer of 2143  $\text{\AA}^2$  [2] (14% of the accessible surface of KaiB and KaiC; Table S1). The second best model with KaiB interacting with KaiCII has a less favorable nonbonded interaction energy ( $-226$  kcal/mol). Among the set of eight models that have KaiB interacting with KaiCI, there are three potentially favorable models (9, 11, and 13) based on the nonbonded interaction energy ( $-305$  to  $-367$  kcal/mol). However, visual examination of these models showed that KaiB interacted predominantly with a highly flexible loop on the CI surface of KaiC (amino acids 112–121) and did not form a large interaction surface with KaiC. All of the models with KaiB interacting with KaiCI had buried accessible areas of less than 1418  $\text{\AA}^2$  ( $<9\%$  of the accessible surface of KaiB and KaiC; Table S1). Consideration of both the nonbonded interaction energy and the buried accessible surface area led us to choose model 1 as the most likely KaiBC model consistent with both the cryoEM

density and the EM gold labeling study showing that KaiB binds to the CII side of KaiC [35].

The robustness of the KaiBC interface indicated by model 1 was tested by rotating the KaiB monomer  $\pm 10^\circ$  and re-running the MDFF simulations. In both cases, the long  $\alpha$ -helices of KaiB returned to essentially the same positions relative to the KaiCII surface and reformed the majority of the same residue–residue interactions with KaiC (Table S2). The robustness of the protein interface provides support for the selection of model 1 as a reasonable model for the KaiBC interaction.

### KaiB monomers form a continuous ring in the KaiBC complex

The selected MDFF-refined model for KaiBC has a KaiB monomer interacting predominantly with one subunit of the KaiC hexamer and partially covering one ATP binding cleft on the KaiCII surface (Figs. 3

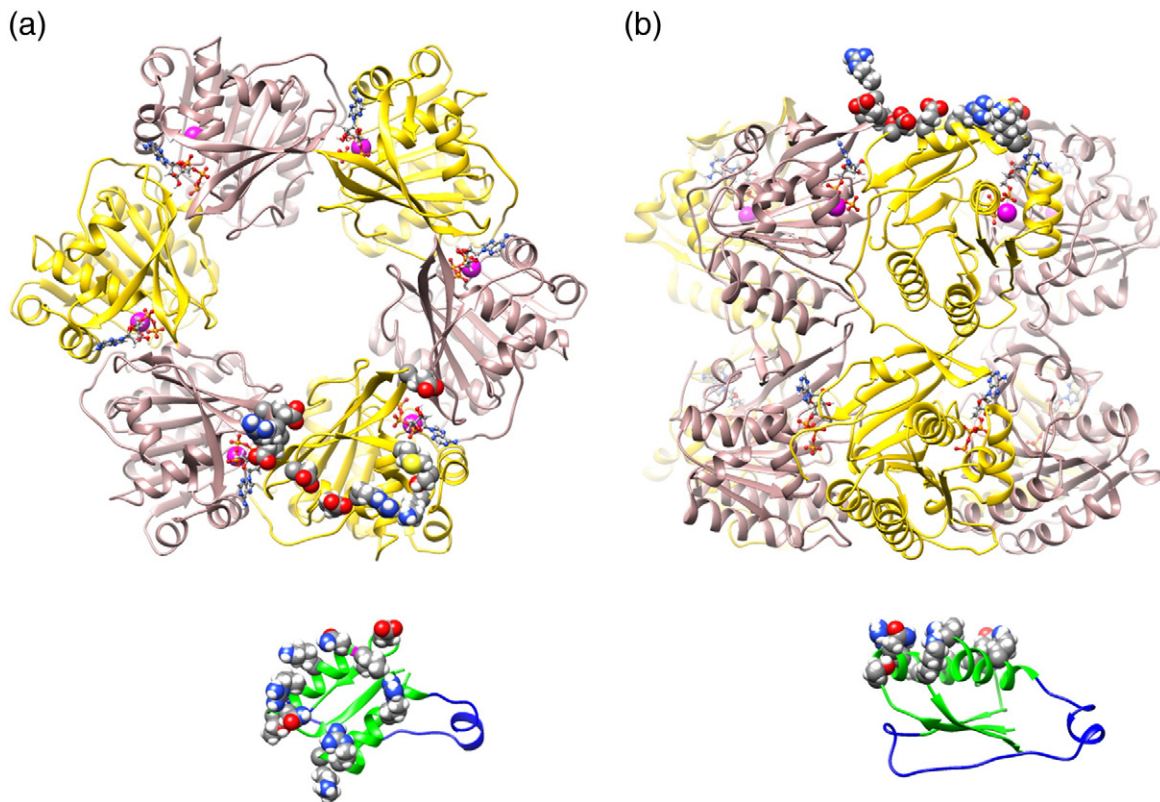


**Fig. 4.** Interaction residues at the KaiBC interface. (a) Top views of the interacting KaiC and KaiB surfaces. The top 10 most strongly interacting residues for both KaiC (K475-chain A, D464-chain A, E272-chain A, E444-chain F, E448-chain F, R269-chain A, R446-chain F, S473-chain A, E448-chain A, M471-chain A) and KaiB (R82, R22, K25, E34, R74, N29, N19, K84, T17, I30) as indicated by the MDFF simulation are shown in space-filling representation. The ATP molecules are shown in ball-and-stick representation and  $Mg^{2+}$  are magenta spheres. KaiB and KaiC are colored as in Fig. 3a. (b) Side views of interacting surfaces.

and 4). During the MDFF simulation, the KaiB dimerization loop (amino acids 45–60) and adjacent short  $\alpha$ -helix (amino acids 61–67) changed conformation to better fit the cryoEM density. In the process, the short  $\alpha$ -helix moved into density corresponding to a neighboring KaiB subunit (Fig. 3a). The cryoEM structure indicates that KaiB binds KaiC as a monomer. It seems reasonable that there would be a conformational change of the KaiB dimerization loop after binding of KaiB to KaiC; however, this is difficult to model in the absence of a high-resolution structure of a KaiB monomer. Therefore, we removed the dimerization loop and short  $\alpha$ -helix (amino acids 45–69) of KaiB before building a KaiBC model with six KaiB monomers. An MDFF simulation with six KaiB monomers docked on the KaiC hexamer indicates that a model with six KaiB monomers bound to the CI side of KaiC is consistent with the cryoEM density (Fig. 3b). The simulation also indicates that neighboring KaiB monomers are closely packed and form a continuous ring around the top of KaiC, further blocking the ATP binding clefts on the KaiCII surface. In fact, the modeled KaiB orientation places the N- and C-termini of each

KaiB monomer in a position to interact with the neighboring KaiB monomer and potentially stabilize the KaiB ring (Fig. 3b).

#### Key interaction residues at the KaiBC interface

The MDFF simulations indicate that the top 10 interaction residues on both KaiB and KaiC are mostly charged residues on the  $\alpha$ -helices of KaiB and the CII surface of KaiC (Fig. 4). On KaiC, the top interaction sites include residues on two adjacent KaiC subunits spanning an ATP binding cleft on the KaiCII surface. On KaiB, the top interaction residues are in the two long  $\alpha$ -helices or within four residues of these helices. The MDFF-refined coordinates for the KaiBC interaction indicate that the core of one KaiB monomer sits mostly on one KaiC subunit and also overlaps with the adjacent clockwise KaiC subunit when viewed from the KaiCII surface (Fig. 4a). Although the KaiB N- and C-termini were not included during the MDFF simulation, they are positioned in such a manner that they could interact with the adjacent counterclockwise KaiC subunit.

If the predicted binding interface on KaiC is correct, then mutations on the KaiCII surface should affect KaiB binding. We have previously mutated KaiC residue R468 into a Cys (KaiC-R468C) [48]. Native gel electrophoresis shows that KaiB binds to both wild-type KaiC and KaiC-R468C; however, the affinity of KaiB for KaiC is slightly higher with the R468C mutant (Fig. 5). Bioluminescence rhythm assays of the circadian clock performed with a cyanobacterial strain lacking the endogenous *kaiC* gene and expressing wild-type KaiC or KaiC-R468C indicate a long period (~55 h) for KaiC-R468C [48]. If the R468C mutation increases the stability of the KaiBC interaction such that KaiB forms a more stable ring on KaiC, this would be consistent with a longer period phenotype as it would presumably take longer for KaiB to dissociate. KaiC residue 468 is within the middle of the predicted KaiBC interface and between the two  $\alpha$ -helices of KaiB (Fig. 5c). The MDFF-based model of the KaiBC interaction presented here will be useful to guide future mutagenesis experiments to probe the KaiBC interface.

## Discussion

A high-resolution structure of the KaiBC complex would be helpful in understanding the mechanistic underpinnings of the cyanobacterial circadian clock. In the absence of a crystal structure for the complex, we pursued a cryoEM structure of the complex and analyzed it with atomic structures for KaiB and KaiC and MDFF-guided molecular dynamics. We used a truncated form of KaiC (KaiC- $\Delta$ 489) in an attempt to make more uniform KaiBC complexes for a cryoEM structural study. However, the KaiB–KaiC- $\Delta$ 489 complexes display compositional heterogeneity with variation in KaiB occupancy, and they may have conformational heterogeneity as well. Even the KaiC hexamer alone does not possess exact 6-fold symmetry, as noted in the crystal structure [22,24]. The dynamic nature of KaiC subunit exchange, which occurs at a higher rate when KaiB is bound, could lead to even greater asymmetry and structural variability for the KaiBC complex. All of these factors may have contributed to the determination of a cryoEM structure at only moderate (16 Å) resolution, despite a relatively large data set of ~195,000 particle images.

The cryoEM structure was analyzed by MDFF simulations with 16 different starting orientations for KaiB. One KaiBC model was selected on the basis of the calculated nonbonded interaction energy and the buried accessible surface area. In the selected model, the two long  $\alpha$ -helices of KaiB form the main interaction surface with KaiC. These helices are accessible in both the dimeric and tetrameric forms of KaiB (Fig. S3). Therefore, while KaiB may initially

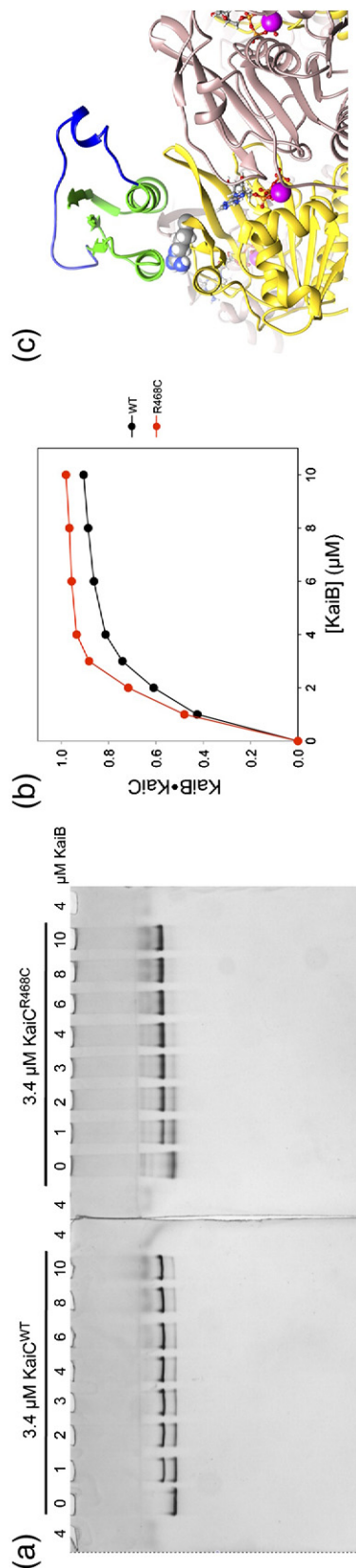


**Fig. 5.** KaiC mutation near the predicted KaiBC interface affects KaiB binding. (a) Native gels showing the interaction of KaiB with wild-type KaiC (left) and KaiC with the R468C mutation (right). (b) Binding curves showing a higher affinity of KaiB for KaiC-R468C. (c) Close-up view of the KaiBC model with KaiC R468 shown in a space-filling representation.

contact KaiC as a dimer, the relatively strong predicted nonbonded interactions between the  $\alpha$ -helices of both KaiB monomers with the CII surface of KaiC could lead to conversion of the dimer into two neighboring monomers bound to KaiC. Each monomer of KaiB would then form the same interactions with adjacent KaiC subunits. The MDFF simulations also indicate that a significant percentage (14%) of the total accessible surface area of KaiB and KaiC is buried when KaiB binds to the CII side of KaiC. This was not the case for the simulations that involved docking KaiB on the CI side of KaiC. Therefore, although KaiB may transiently bind to multiple sites on KaiC, this cryoEM and MDFF study supports the earlier EM gold labeling study of KaiB in complex with KaiC, indicating that KaiB binds to KaiCII [35].

The cryoEM and MDFF-based model for the KaiBC complex offers an explanation for the finding that truncation of the C-terminal tails of *T. elongatus* KaiB increases the binding affinity of KaiB for KaiC [37]. In the selected KaiBC model, the N- and C-terminal tails of KaiB are in a position to interact with a neighboring KaiB monomer bound to KaiC. However, this also means that if fewer than six KaiB monomers are bound to KaiC, the long C-terminal tails of KaiB (amino acids 94–102 for *S. elongatus*, amino acids 95–108 for *T. elongatus*) could block access to the remaining KaiC subunits. The KaiBC model also provides a rationale for how KaiB promotes the dephosphorylation of KaiC. The model shows that one KaiB monomer binds to two KaiC subunits and covers one ATP binding cleft on KaiCII. A complete ring of six bound KaiB monomers would cover all of the ATP binding clefts on this side of KaiC. The dephosphorylation mechanism of KaiC has been shown to involve a reversal of the phosphorylation reaction that places the phosphates from KaiC back onto ADP [13,14]. Covering the ATP binding clefts would presumably block the entry of ADP and the release of ATP and stall the dephosphorylation reaction.

In summary, our goal was to gain more detailed structural information on the interaction of KaiB with KaiC. The cryoEM structure shows that KaiB forms a continuous ring of density on one side of KaiC. The MDFF analysis indicates that the ring of KaiB density is consistent with six monomers bound to the CII side of a KaiC hexamer. The cryoEM and MDFF results led us to propose an atomic model for the KaiBC complex with each of the six KaiB monomers covering an ATP binding cleft on the CII side of KaiC. The biological function of KaiB is to push KaiC toward a dephosphorylated state in the cyanobacterial posttranslational circadian oscillator by opposing the action of KaiA. The KaiBC model presented here suggests a possible way in which KaiB could influence the ATP binding pockets within the CII ring of KaiC.

## Materials and Methods

### Expression and purification of wild-type KaiB and KaiC- $\Delta$ 489

The glutathione S-transferase (GST)-KaiB and GST-KaiC fusion proteins were expressed in *Escherichia coli* and purified by affinity chromatography followed by GST cleavage with PreScission protease (GE Healthcare) by gel-filtration chromatography as described in Refs. [41] and [16]. The KaiC- $\Delta$ 489 and KaiC-R468C proteins were expressed as GST fusion proteins in *E. coli* DH5 $\alpha$  cells and purified by affinity chromatography with glutathione agarose beads (Thermo Scientific) following GST cleavage with recombinant GST-human rhinovirus 3C protease and ion-exchange chromatography.

### X-ray crystallography

Crystals for *S. elongatus* KaiB were grown from droplets containing 6.5 mg/mL KaiB–KaiC complex, 20 mM Tris (pH 7.8), 100 mM NaCl, 5 mM MgCl<sub>2</sub>, 1 mM ATP, and 2 mM  $\beta$ -mercaptoethanol. The reservoir solution was 100 mM sodium acetate, 500 mM sodium formate, and 5% glycerol (v/v). Crystals grew within a week at room temperature using the hanging vapor diffusion technique. They were mounted in nylon loops, cryo-protected in mother liquor containing 25% glycerol (v/v), and then flash frozen in liquid nitrogen. X-ray diffraction data were collected on the 21-ID-D beamline of the Life Sciences Collaborative Access Team at the Advanced Photon Source, Argonne National Laboratory (Argonne, IL). Data were integrated and scaled with the program HKL2000 [49]. The structure was determined by the molecular replacement technique using the program MOLREP [50,51] and the *T. elongatus* KaiB structure with PDB 2QKE (dimer) as the search model. Initial refinement was carried out with the program BUSTER-TNT [52] and N- and C-terminal residues for the four subunits were gradually built into the electron density, followed by additional rounds of refinement with the program PHENIX [53]. The program Coot [54] was used for manual rebuilding. Water molecules were added gradually and isotropic/TLS refinement was continued with the program PHENIX with intermittent adjustments of side-chain torsion angles. A summary of crystal data, data collection, and refinement parameters is provided in Table 1. Illustrations were generated with the program UCSF Chimera [47].

### Cryo-electron microscopy

KaiB–KaiC- $\Delta$ 489 complexes were formed for EM studies as previously described for wild-type *S. elongatus* KaiB and KaiC [16]. KaiB–KaiC- $\Delta$ 489 samples were applied to freshly prepared EM grids with homemade holey carbon film and to C-flat grids (Protochips, Inc.). After blotting with filter paper, the sample grid was plunged into ethane slush cooled by liquid nitrogen with either a homebuilt plunger or a Vitrobot (FEI Company). CryoEM images were collected on an FEI Polara microscope (300 kV, FEG) operated at liquid nitrogen temperature and using a Gatan UltraScan 4000 CCD camera. The majority

of the data (159,952 particles) were collected with an absolute magnification of 254,669 $\times$  at 300 kV. An additional smaller set of data (35,274 particles) was collected at 267,493 $\times$  at 200 kV. The defocus range for the entire data set was  $-1$  to  $-7$   $\mu\text{m}$ .

### Image processing

Individual particle images (195,226 total) were picked manually using in-house scripts that utilize EMAN sub-routines [55], and the stacks were subsequently binned to a pixel size of 2.32  $\text{\AA}$  for the majority of the data set (2.21  $\text{\AA}$  for the smaller subset). At the start of refinement, the initial estimates for microscope defocus and astigmatism parameters were calculated with CTFFIND3 [56]. The images were filtered, normalized, and band-pass filtered between 140 and 10  $\text{\AA}$  for MSA classification in IMAGIC [57]. During the MSA-CLASSIFY step, the worst 15% of the images were ignored. The majority of the data set (159,952 particles) were classified into 2000 class averages from which a subset of 360 class averages representing side views was selected. This subset was subjected to an Eigenimage analysis following a procedure applied to GroEL [39]. First, the selected side-view class averages were rotationally and translationally aligned, forming a reference set. Then, the particle images that formed the side-view class averages (21,937 particles) were extracted and rotationally and translationally aligned to the reference set. The aligned particle images underwent a round of MSA classification. One of the resulting eigenimages (Fig. S7) described the presence or absence of a third layer of KaiB in the particle images. This eigenimage was used for sorting the 255,000 $\times$  side-view particle images into two groups, one with high KaiB occupancy (12,527 particles) and the other with low KaiB occupancy (9410 particles). A similar Eigenimage analysis was performed on the data set collected with a magnification of 267,000 $\times$ , and this resulted in smaller subgroups of side-view particle images with high KaiB occupancy (425 particles) and low KaiB occupancy (496 particles).

The larger 255,000 $\times$  subgroups underwent MSA classification, resulting in 1200 and 900 class averages for the high and low KaiB occupancy sets, respectively. Each set of class averages was processed with the 3D Fourier Space programs developed by Rubinstein that incorporate the gold standard refinement scheme† [58]. The initial starting model for both sets was a 30- $\text{\AA}$  filtered representation of the KaiC- $\Delta$ 489 hexamer (amino acids 14–489). A third layer of KaiB density emerged in the structure for the set with high KaiB occupancy but not for the set with low KaiB occupancy (Fig. S5). Although no symmetry was imposed, the third layer of KaiB density appeared approximately 6-fold symmetric in the high KaiB occupancy structure (Fig. S5). The refined class-average-based structure with high KaiB occupancy had a gold standard resolution of 29  $\text{\AA}$  at the FSC 0.5 threshold (21  $\text{\AA}$  at the 0.143 threshold). This class-average-based structure was used as the starting model for a systematic parameter search of the 12,527 particles in the high KaiB occupancy subgroup. After five rounds of refinement, the KaiB density still appeared approximately 6-fold symmetric (Fig. S5). Therefore, the structure at the end of round five was rotated so that the 6-fold axis was along the z-axis, and a second systematic parameter search was performed. The

cross-correlation (cc) values of the resulting parameter file were converted into Frealign style phase residuals (phase residual =  $100 - \text{cc value}$ ), and a C6 symmetrized map was calculated using FREALIGN [59] in iflag = 0 mode. Additional rounds of refinement were performed using the 3D Fourier Space programs and with C6 symmetric odd and even maps calculated with FREALIGN at the end of each round. This refined particle-image-based structure based on 11,415 particles had a gold standard resolution of 18  $\text{\AA}$  at the FSC 0.5 threshold (16  $\text{\AA}$  at the FSC 0.143 threshold).

The refined particle-image-based structure was used as the starting model for a systematic parameter search with all 159,952 particles collected with a magnification of 255,000 $\times$  and all 35,274 particles collected at 267,000 $\times$ . The voxel size of the search model was appropriately adjusted for the 267,000 $\times$  data set with PROC3D in EMAN [55]. The selected particles from the two data sets with different magnifications were combined into one map using FREALIGN with the relmag parameter (relative magnification correction factor). Three different relmag values were tried, 0.99, 1.0, and 1.01. The best FSC curve was found with a relmag value of 1.0. The final map shown in Fig. 2 is C6 symmetrized, based on 98,932 particles (51% of 195,226 total particles), sharpened with a  $B$ -factor of  $-1000 \text{\AA}^2$  and filtered with the Cref filter [60]. The resolution of the final map is 16  $\text{\AA}$  at the FSC 0.5 threshold and 13  $\text{\AA}$  at the FSC 0.143 threshold. The lowest spatial frequency used during 3D Fourier Space refinement was 140  $\text{\AA}$ . The highest spatial frequency was started at 30  $\text{\AA}$  in the initial round and maintained at two resolution shells below the resolution limit of the map, as assessed by FSC with the 0.143 criterion. The cryoEM structure has been deposited in the EM Data Bank EMD: 5672.

### MDFF simulations

In preparation for MDFF simulations, an atomic model was generated for a C-terminally truncated form of *S. elongatus* KaiC- $\Delta$ 489 starting with the crystal structure of the KaiC hexamer (PDB ID: 3DVL) and removing coordinates for the C-terminal tails (amino acids 490–519). Two copies of Ser431 were computationally modified to the phosphorylated state with VMD 1.9 [40] so that all Ser431 and all Thr432 residues were phosphorylated for the MDFF simulations. All 12 ATP molecules were retained in the structure for the simulations. An atomic model was generated for an *S. elongatus* KaiB monomer from the X-ray crystallographic coordinates. Given the observed flexibility for the *S. elongatus* KaiB C-terminal tails, the MDFF simulations were performed with a computationally C-terminally truncated form of the KaiB monomer containing residues 7–93 from chain A of the crystal structure.

The MDFF plugin for NAMD 2.8 and VMD 1.9 [40,43,44] was used to perform molecular dynamics simulations guided by the cryoEM density map. The MDFF simulations were performed with implicit solvent, the CHARMM force field, and a gscale factor of 0.3, which describes the strength of the external potential derived from the EM density map. The KaiC- $\Delta$ 489 hexamer coordinates were docked into the cryoEM density in two different orientations, with the CI or CII ring toward KaiB, with UCSF Chimera [47]. MDFF simulations (100 ps each) were

performed for both KaiC orientations, first in the absence of KaiB. Ten residues at the C-terminal end of KaiC moved into the KaiB density ring when KaiC was oriented with the CII ring toward KaiB, so these residues (amino acids 480–489) were computationally removed before the MDFF simulations with KaiB.

Eight different orientations of the KaiB monomer, four with the KaiB helices oriented toward KaiC and four with the KaiB  $\beta$ -stands oriented toward KaiC, were tested with each KaiC orientation. The four helix-down KaiB orientations and the four strand-down KaiB orientations were related by 90°. Visual assessment with UCSF Chimera [47] of the KaiBC models and the cryoEM density indicated that the helix-down orientations more closely resembled the cryoEM density than the strand-down orientations. In addition, models with other KaiB monomer surfaces docked next to KaiC did not fit the cryoEM density as well. The initial KaiBC coordinates were docked into the cryoEM density with UCSF Chimera [47], leaving a small ~5-Å gap between KaiB and KaiC. One-hundred-picosecond MDFF simulations were performed followed by 2000 steps of minimization. After the selection of one KaiBC model, two additional 100-ps MDFF simulations were performed with KaiB rotated by  $\pm 10^\circ$  from its selected binding orientation and raised ~5 Å above the KaiC surface so that the protein interface would be reformed during the simulation. Finally, one MDFF simulation was performed with six docked KaiB monomers in the selected KaiB binding orientation, with KaiB raised ~5 Å above the KaiC surface, and with the KaiB dimerization loop and short helix (amino acids 45–69) computationally removed to avoid steric clashes with neighboring KaiB monomers. The intermolecular non-bonded interaction energies between KaiC and KaiB subunits were evaluated with the NAMD Energy plugin in VMD [40] and the buried accessible surface area was measured with UCSF Chimera [47]. The MDFF simulations were performed on the Case Western Reserve University High Performance Computing Cluster.

### KaiC R468C mutant binding assays

The KaiC-R468C mutant was first described by Xu *et al.* [48]. The binding reactions between KaiB and KaiC proteins were carried out at 3.4  $\mu$ M of the wild type or KaiC-R468C with various concentrations (0–10  $\mu$ M) of the wild-type KaiB in 20 mM Tris–HCl, pH 8, 150 mM NaCl, 5 mM MgCl<sub>2</sub>, 1 mM ATP, and 0.5 mM ethylenediaminetetraacetic acid at 30 °C for 4 h. Native polyacrylamide gel electrophoresis was performed as previously described [61].

### Accession numbers

Final coordinates and structure factors for the KaiB crystal structure have been deposited in the PDB with accession number 4KSO.

### Acknowledgements

We would like to thank Mr. Said K. Sidiqi for help with protein expression and purification, Dr. Yao Xu for

providing the expression construct for KaiC R468C, and Dr. Zdzislaw Wawrzak, Northwestern University, for assistance with X-ray diffraction data collection and processing. Use of the Advanced Photon Source was supported by the U.S. Department of Energy, Office of Science, Office of Basic Energy Sciences, under Contract No. DE-AC02-06CH11357. Use of the Life Sciences Collaborative Access Team Sector 21 was supported by the Michigan Economic Development Corporation, and this research program was supported by the Michigan Technology Tri-Corridor (Grant 085P1000817). This work was supported by the National Institutes of Health grants GM067152 (to C.H.J.), GM073845 (to M.E.), and GM081646 (to P.L.S.).

### Supplementary Data

Supplementary data to this article can be found online at <http://dx.doi.org/10.1016/j.jmb.2013.06.018>

Received 19 March 2013;

Received in revised form 18 May 2013;

Accepted 11 June 2013

Available online 22 June 2013

### Keywords:

circadian oscillator;  
cryoEM;  
MDFF;  
protein–protein interface;  
Synechococcus elongatus

Present address: D.R. Williams, Department of Pathology and Laboratory Medicine, University of Pennsylvania School of Medicine, Philadelphia, PA 19104, USA.

† [www.sickkids.ca/research/rubinstein](http://www.sickkids.ca/research/rubinstein)

### Abbreviations used:

cryoEM, cryo-electron microscopy; EM, electron microscopy; FSC, Fourier shell correlation; GST, glutathione *S*-transferase; MDFF, molecular dynamics flexible fitting; PDB, Protein Data Bank; PTO, posttranslational oscillator; SAXS, small-angle X-ray scattering.

### References

- [1] Egli E, Johnson CH. A circadian clock nanomachine that runs without transcription or translation. *Curr Opin Neurobiol* 2013. In press. <http://dx.doi.org/10.1016/j.conb.2013.02.012>.
- [2] Rust MJ, Golden SS, O'Shea EK. Light-driven changes in energy metabolism directly entrain the cyanobacterial circadian oscillator. *Science* 2011;331:220–3.
- [3] Nakajima M, Imai K, Ito H, Nishiwaki T, Murayama Y, Iwasaki H, et al. Reconstitution of circadian oscillation of cyanobacterial KaiC phosphorylation in vitro. *Science* 2005;308:414–5.

- [4] Ito H, Kageyama H, Mutsuda M, Nakajima M, Oyama T, Kondo T. Autonomous synchronization of the circadian KaiC phosphorylation rhythm. *Nat Struct Mol Biol* 2007;14:1084–8.
- [5] Terauchi K, Kitayama Y, Nishiwaki T, Miwa K, Murayama Y, Oyama T, et al. ATPase activity of KaiC determines the basic timing for circadian clock of cyanobacteria. *Proc Natl Acad Sci USA* 2007;104:16377–81.
- [6] Johnson CH, Egli M, Stewart PL. Structural insights into a circadian oscillator. *Science* 2008;322:697–701.
- [7] Johnson CH, Stewart PL, Egli M. The cyanobacterial circadian system: from biophysics to bioevolution. *Annu Rev Biophys* 2011;40:143–67.
- [8] Nishiwaki T, Satomi Y, Kitayama Y, Terauchi K, Kiyohara R, Takao T, et al. A sequential program of dual phosphorylation of KaiC as a basis for circadian rhythm in cyanobacteria. *EMBO J* 2007;26:4029–37.
- [9] Rust MJ, Markson JS, Lane WS, Fisher DS, O'Shea EK. Ordered phosphorylation governs oscillation of a three-protein circadian clock. *Science* 2007;318:809–12.
- [10] Bretschneider C, Rose RJ, Hertel S, Axmann IM, Heck AJ, Kollmann M. A sequestration feedback determines dynamics and temperature entrainment of the KaiABC circadian clock. *Mol Syst Biol* 2010;6:389.
- [11] Pattanayek R, Williams DR, Rossi G, Weigand S, Mori T, Johnson CH, et al. Combined SAXS/EM based models of the *S. elongatus* post-translational circadian oscillator and its interactions with the output His-kinase SasA. *PLoS One* 2011;6:e23697.
- [12] Qin X, Byrne M, Mori T, Zou P, Williams DR, McHaourab H, et al. Intermolecular associations determine the dynamics of the circadian KaiABC oscillator. *Proc Natl Acad Sci USA* 2010;107:14805–10.
- [13] Egli M, Mori T, Pattanayek R, Xu Y, Qin X, Johnson CH. Dephosphorylation of the core clock protein KaiC in the cyanobacterial KaiABC circadian oscillator proceeds via an ATP synthase mechanism. *Biochemistry* 2012;51:1547–58.
- [14] Nishiwaki T, Kondo T. Circadian autodephosphorylation of cyanobacterial clock protein KaiC occurs via formation of ATP as intermediate. *J Biol Chem* 2012;287:18030–5.
- [15] Kageyama H, Nishiwaki T, Nakajima M, Iwasaki H, Oyama T, Kondo T. Cyanobacterial circadian pacemaker: Kai protein complex dynamics in the KaiC phosphorylation cycle in vitro. *Mol Cell* 2006;23:161–71.
- [16] Mori T, Williams DR, Byrne MO, Qin X, Egli M, McHaourab HS, et al. Elucidating the ticking of an in vitro circadian clockwork. *PLoS Biol* 2007;5:e93.
- [17] van Zon JS, Lubensky DK, Altana PR, ten Wolde PR. An allosteric model of circadian KaiC phosphorylation. *Proc Natl Acad Sci USA* 2007;104:7420–5.
- [18] Hanaoka M, Takai N, Hosokawa N, Fujiwara M, Akimoto Y, Kobori N, et al. RpaB, another response regulator operating circadian clock-dependent transcriptional regulation in *Synechococcus elongatus* PCC 7942. *J Biol Chem* 2012;287:26321–7.
- [19] Iwasaki H, Williams SB, Kitayama Y, Ishiura M, Golden SS, Kondo T. A kaiC-interacting sensory histidine kinase, SasA, necessary to sustain robust circadian oscillation in cyanobacteria. *Cell* 2000;101:223–33.
- [20] Takai N, Nakajima M, Oyama T, Kito R, Sugita C, Sugita M, et al. A KaiC-associating SasA–RpaA two-component regulatory system as a major circadian timing mediator in cyanobacteria. *Proc Natl Acad Sci USA* 2006;103:12109–14.
- [21] Pattanayek R, Mori T, Xu Y, Pattanayek S, Johnson CH, Egli M. Structures of KaiC circadian clock mutant proteins: a new phosphorylation site at T426 and mechanisms of kinase, ATPase and phosphatase. *PLoS One* 2009;4:e7529.
- [22] Pattanayek R, Williams DR, Pattanayek S, Xu Y, Mori T, Johnson CH, et al. Analysis of KaiA–KaiC protein interactions in the cyano-bacterial circadian clock using hybrid structural methods. *EMBO J* 2006;25:2017–28.
- [23] Phong C, Markson JS, Wilhoite CM, Rust MJ. Robust and tunable circadian rhythms from differentially sensitive catalytic domains. *Proc Natl Acad Sci USA* 2013;110:1124–9.
- [24] Pattanayek R, Wang J, Mori T, Xu Y, Johnson CH, Egli M. Visualizing a circadian clock protein: crystal structure of KaiC and functional insights. *Mol Cell* 2004;15:375–88.
- [25] Ye S, Vakonakis I, Ioege TR, LiWang AC, Sacchettini JC. Crystal structure of circadian clock protein KaiA from *Synechococcus elongatus*. *J Biol Chem* 2004;279:20511–8.
- [26] Egli M, Pattanayek R, Sheehan JH, Xu Y, Mori T, Smith JA, et al. Loop–loop interactions regulate KaiA-stimulated KaiC phosphorylation in the cyanobacterial KaiABC circadian clock. *Biochemistry* 2013;52:1208–20.
- [27] Kim YI, Dong G, Carruthers Jr CW, Golden SS, LiWang A. The day/night switch in KaiC, a central oscillator component of the circadian clock of cyanobacteria. *Proc Natl Acad Sci USA* 2008;105:12825–30.
- [28] Vakonakis I, LiWang AC. Structure of the C-terminal domain of the clock protein KaiA in complex with a KaiC-derived peptide: implications for KaiC regulation. *Proc Natl Acad Sci USA* 2004;101:10925–30.
- [29] Kitayama Y, Iwasaki H, Nishiwaki T, Kondo T. KaiB functions as an attenuator of KaiC phosphorylation in the cyanobacterial circadian clock system. *EMBO J* 2003;22:2127–34.
- [30] Garces RG, Wu N, Gillon W, Pai EF. Anabaena circadian clock proteins KaiA and KaiB reveal a potential common binding site to their partner KaiC. *EMBO J* 2004;23:1688–98.
- [31] Hitomi K, Oyama T, Han S, Arvai AS, Getzoff ED. Tetrameric architecture of the circadian clock protein KaiB. A novel interface for intermolecular interactions and its impact on the circadian rhythm. *J Biol Chem* 2005;280:19127–35.
- [32] Iwase R, Imada K, Hayashi F, Uzunaki T, Morishita M, Onai K, et al. Functionally important substructures of circadian clock protein KaiB in a unique tetramer complex. *J Biol Chem* 2005;280:43141–9.
- [33] Pattanayek R, Williams DR, Pattanayek S, Mori T, Johnson CH, Stewart PL, et al. Structural model of the circadian clock KaiB–KaiC complex and mechanism for modulation of KaiC phosphorylation. *EMBO J* 2008;27:1767–78.
- [34] Akiyama S, Nohara A, Ito K, Maeda Y. Assembly and disassembly dynamics of the cyanobacterial periodosome. *Mol Cell* 2008;29:703–16.
- [35] Pattanayek R, Yadagirib KK, Ohi MD, Egli M. Nature of KaiB–KaiC binding in the cyanobacterial circadian oscillator. *Cell Cycle* 2013;12:810–7.
- [36] Chang YG, Tseng R, Kuo NW, LiWang A. Rhythmic ring–ring stacking drives the circadian oscillator clockwise. *Proc Natl Acad Sci USA* 2012;109:16847–51.
- [37] Murakami R, Mutoh R, Iwase R, Furukawa Y, Imada K, Onai K, et al. The roles of the dimeric and tetrameric structures of the clock protein KaiB in the generation of circadian oscillations in cyanobacteria. *J Biol Chem* 2012;287:29506–15.
- [38] Murayama Y, Mukaiyama A, Imai K, Onoue Y, Tsunoda A, Nohara A, et al. Tracking and visualizing the circadian ticking

- of the cyanobacterial clock protein KaiC in solution. *EMBO J* 2011;30:68–78.
- [39] Clare DK, Vasishtan D, Stagg S, Quispe J, Farr GW, Topf M, et al. ATP-triggered conformational changes delineate substrate-binding and -folding mechanics of the GroEL chaperonin. *Cell* 2012;149:113–23.
- [40] Humphrey W, Dalke A, Schulten K. VMD: visual molecular dynamics. *J Mol Graph* 1996;14(33–38):27–38.
- [41] Nishiwaki T, Satomi Y, Nakajima M, Lee C, Kiyohara R, Kageyama H, et al. Role of KaiC phosphorylation in the circadian clock system of *Synechococcus elongatus* PCC 7942. *Proc Natl Acad Sci USA* 2004;101:13927–32.
- [42] Xu Y, Mori T, Pattanayek R, Pattanayek S, Egli M, Johnson CH. Identification of key phosphorylation sites in the circadian clock protein KaiC by crystallographic and mutagenetic analyses. *Proc Natl Acad Sci USA* 2004;101:13933–8.
- [43] Trabuco LG, Villa E, Mitra K, Frank J, Schulten K. Flexible fitting of atomic structures into electron microscopy maps using molecular dynamics. *Structure* 2008;16:673–83.
- [44] Trabuco LG, Villa E, Schreiner E, Harrison CB, Schulten K. Molecular dynamics flexible fitting: a practical guide to combine cryo-electron microscopy and X-ray crystallography. *Methods* 2009;49:174–80.
- [45] Chan KY, Trabuco LG, Schreiner E, Schulten K. Cryo-electron microscopy modeling by the molecular dynamics flexible fitting method. *Biopolymers* 2012;97:678–86.
- [46] Doronin K, Flatt JW, Di Paolo NC, Khare R, Kalyuzhnyi O, Acchione M, et al. Coagulation factor X activates innate immunity to human species C adenovirus. *Science* 2012;338:795–8.
- [47] Pettersen EF, Goddard TD, Huang CC, Couch GS, Greenblatt DM, Meng EC, et al. UCSF Chimera—a visualization system for exploratory research and analysis. *J Comput Chem* 2004;25:1605–12.
- [48] Xu Y, Mori T, Johnson CH. Cyanobacterial circadian clockwork: roles of KaiA, KaiB and the kaiBC promoter in regulating KaiC. *EMBO J* 2003;22:2117–26.
- [49] Otwinowski Z, Minor W. Processing of X-ray diffraction data collected in oscillation mode. In: Carter CWJ, Sweet RM, R. M., editors. *Methods in enzymology: macromolecular crystallography, part A*, Vol. 276. USA: Elsevier; 1997. p. 307–26.
- [50] CCP4. The CCP4 suite: programs for protein crystallography. *Acta Crystallogr Sect D Biol Crystallogr* 1994;50:760–3.
- [51] Vagin A, Teplyakov A. Molecular replacement with MOLREP. *Acta Crystallogr Sect D Biol Crystallogr* 2010;66:22–5.
- [52] Blanc E, Roversi P, Vonrhein C, Flensburg C, Lea SM, Bricogne G. Refinement of severely incomplete structures with maximum likelihood in BUSTER-TNT. *Acta Crystallogr Sect D Biol Crystallogr* 2004;60:2210–21.
- [53] Adams PD, Afonine PV, Bunkoczi G, Chen VB, Davis IW, Echols N, et al. PHENIX: a comprehensive Python-based system for macromolecular structure solution. *Acta Crystallogr Sect D Biol Crystallogr* 2010;66:213–21.
- [54] Emsley P, Cowtan K. Coot: model-building tools for molecular graphics. *Acta Crystallogr Sect D Biol Crystallogr* 2004;60:2126–32.
- [55] Ludtke SJ, Baldwin PR, Chiu W. EMAN: semiautomated software for high-resolution single-particle reconstructions. *J Struct Biol* 1999;128:82–97.
- [56] Mindell JA, Grigorieff N. Accurate determination of local defocus and specimen tilt in electron microscopy. *J Struct Biol* 2003;142:334–47.
- [57] van Heel M, Harauz G, Orlova EV, Schmidt R, Schatz M. A new generation of the IMAGIC image processing system. *J Struct Biol* 1996;116:17–24.
- [58] Benlekbir S, Bueler SA, Rubinstein JL. Structure of the vacuolar-type ATPase from *Saccharomyces cerevisiae* at 11-Å resolution. *Nat Struct Mol Biol* 2012;19:1356–62.
- [59] Grigorieff N. FREALIGN: high-resolution refinement of single particle structures. *J Struct Biol* 2007;157:117–25.
- [60] Rosenthal PB, Henderson R. Optimal determination of particle orientation, absolute hand, and contrast loss in single-particle electron cryomicroscopy. *J Mol Biol* 2003;333:721–45.
- [61] Mori T, Saveliev SV, Xu Y, Stafford WF, Cox MM, Inman RB, et al. Circadian clock protein KaiC forms ATP-dependent hexameric rings and binds DNA. *Proc Natl Acad Sci USA* 2002;99:17203–8.

## **SUPPLEMENTAL INFORMATION**

### **CryoEM and Molecular Dynamics of the Circadian KaiB–KaiC Complex Indicates KaiB Monomers Interact with KaiC and Block ATP Binding Clefs**

Seth A. Villarreal,<sup>1</sup> Rekha Pattanayek,<sup>2</sup> Dewight R. Williams,<sup>3,5</sup> Tetsuya Mori,<sup>4</sup> Ximing Qin,<sup>4</sup> Carl H. Johnson,<sup>4</sup> Martin Egli,<sup>2</sup> and Phoebe L. Stewart<sup>1\*</sup>

<sup>1</sup>Department of Pharmacology and Cleveland Center for Membrane and Structural Biology, Case Western Reserve University, Cleveland, OH 44106, USA

<sup>2</sup>Department of Biochemistry, Vanderbilt University, School of Medicine, Nashville, TN 37232, USA

<sup>3</sup>Department of Molecular Physiology and Biophysics, Vanderbilt University, School of Medicine, Nashville, TN 37232, USA

<sup>4</sup>Department of Biological Sciences, Vanderbilt University, Nashville, TN 37235, USA

<sup>5</sup>Present address: Department of Pathology and Laboratory Medicine, University of Pennsylvania School of Medicine, Philadelphia, PA 19104, USA

\* To whom correspondence should be addressed. Tel: 216-368-4349; Fax: 216-368-1300; Email: phoebe.stewart@case.edu

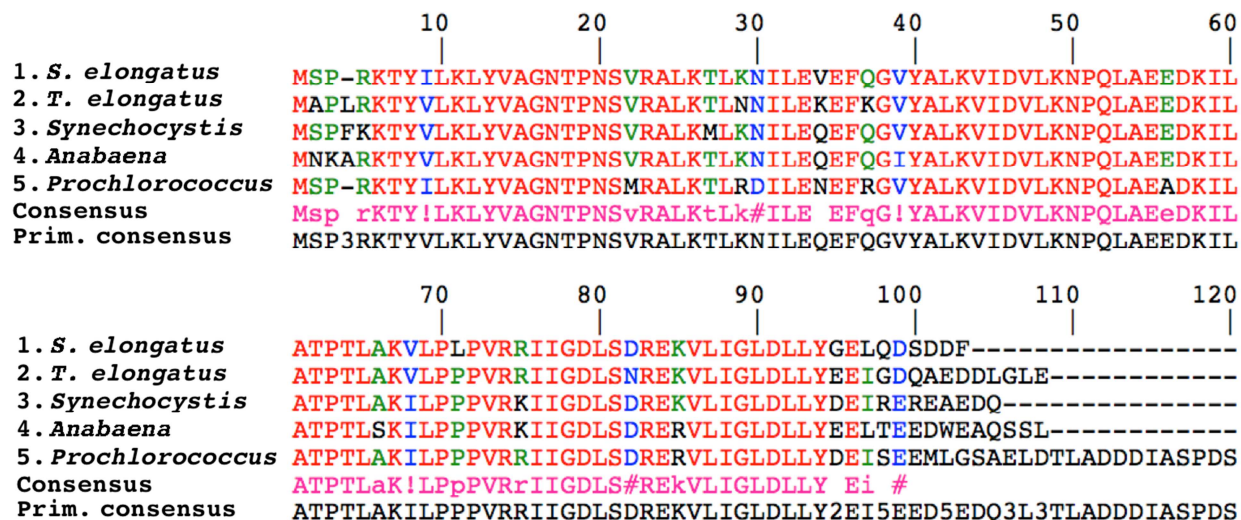


**Figure S1. Sequence alignment for KaiB proteins from selected cyanobacteria.** 1. KaiB *Synechococcus elongatus* PCC 7942, gi|22002534|; 2. KaiB *Thermosynechococcus elongatus* BP-1, gi|22294203|; 3. KaiB *Synechocystis* sp. PCC 6803, gi|16332221|; 4. KaiB *Anabaena variabilis* ATCC 29413, gi|75700965|; 5. KaiB *Prochlorococcus marinus* str. MIT 9313, gi|33863686|. The alignment was performed with the program MULTALIN (Combet et al, 2000; Corpet, 1998). Residues conserved for 90% or more (upper-case letters): 76 (63.33%). Residues conserved for 50% and less than 90% (lower-case letters): 13 (10.83%). Residues conserved less than 50 % (white space): 25 (20.83%). IV conserved positions (!): 3 (2.50%). LM conserved positions (\$): 0. FY conserved positions (%): 0. NDQEBZ conserved positions (#): 3 (2.50%). Numbering of residues in the present contribution refers to the KaiB protein from *T. elongatus* (M1 to E108), i.e. *T. elongatus* Y94 corresponds to *S. elongatus* Y93, Y8 corresponds to Y7, etc.

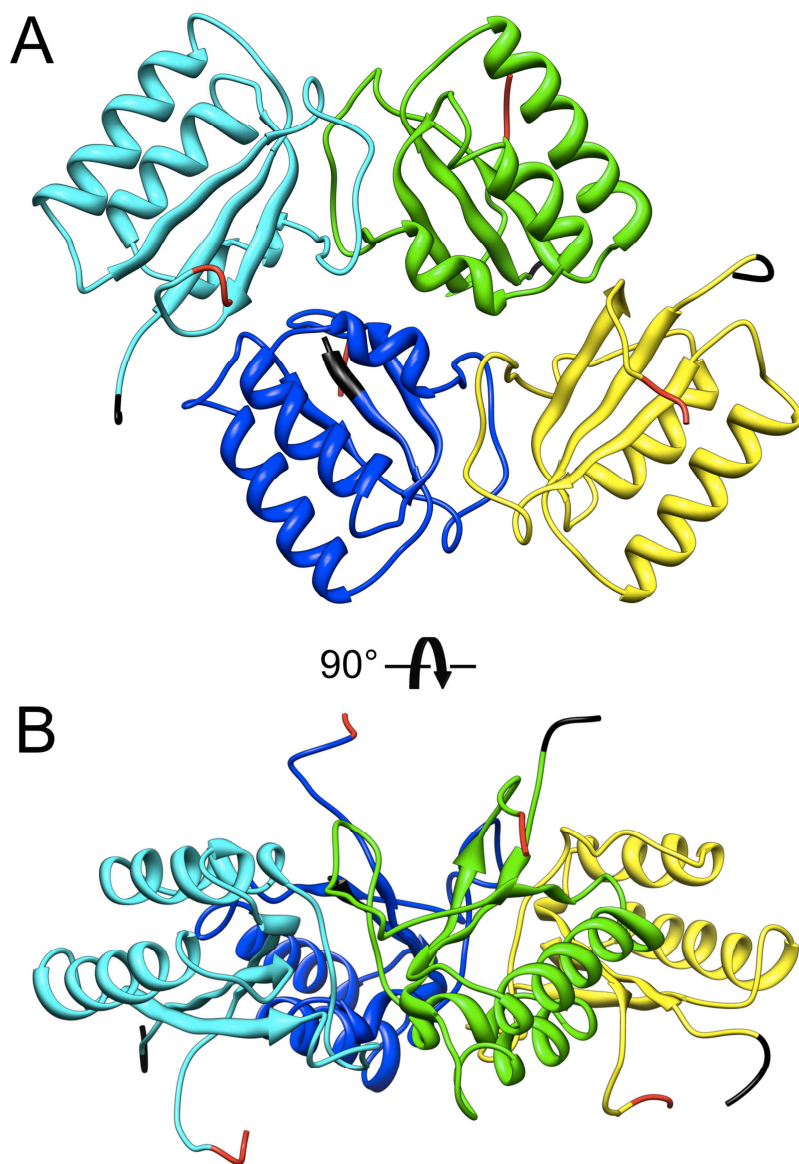


**Figure S2. Conformation of the KaiB tetramer.** The KaiB tetramer viewed **A)** roughly along the non-crystallographic dyad relating the two dimers, and **B)** from the side, after rotating around the horizontal by 90°. Subunits are colored blue (a), yellow (b), green (c) and cyan (d), and ribbons at the N- and C-terminal ends are colored in black and red, respectively. The drawing was generated with the program UCSF Chimera (Pettersen et al, 2004).

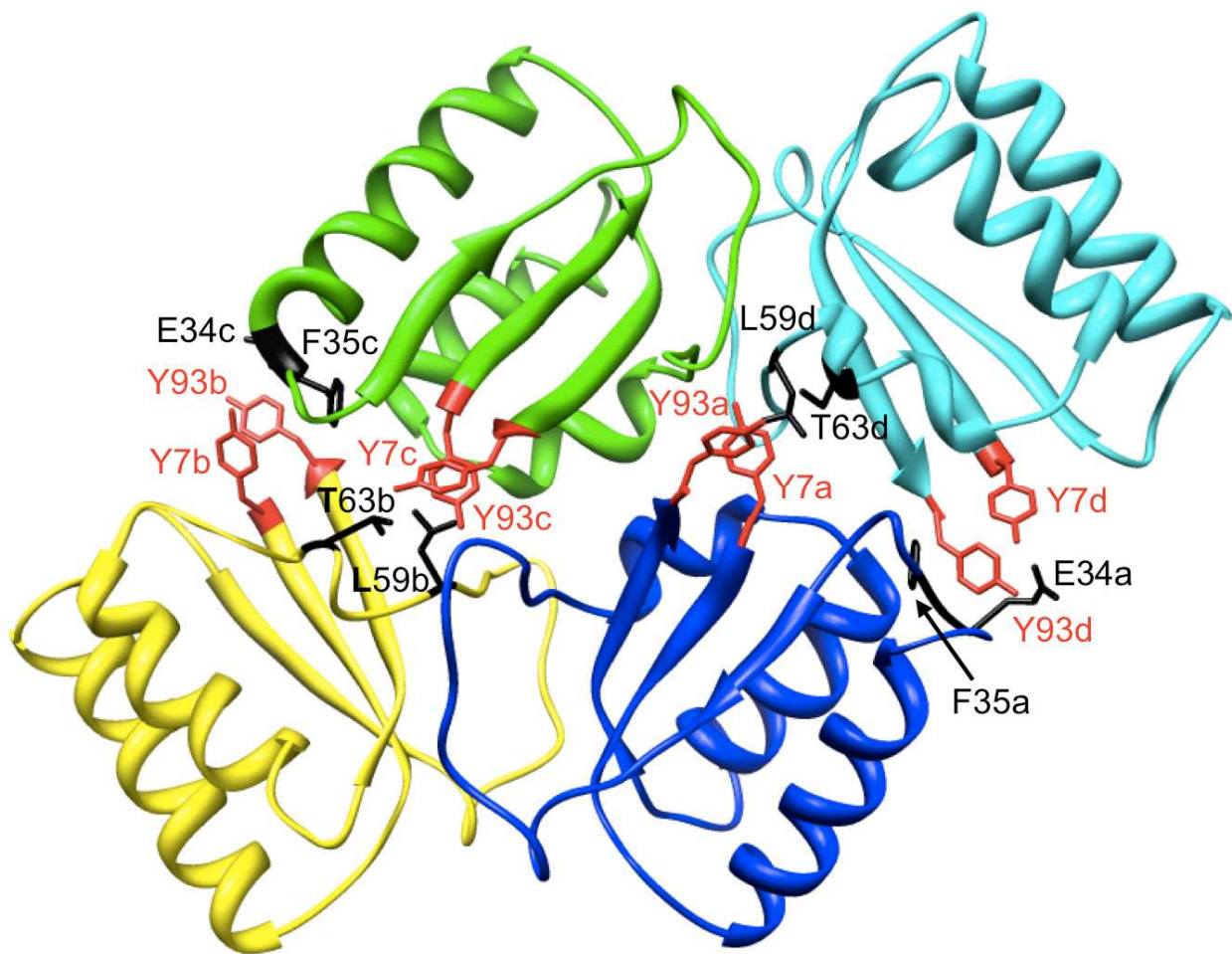


**Figure S3. Interactions stabilizing the KaiB dimer-dimer interface.** Tyrosines 7 and 93 near the N- and C-terminal ends, respectively (side chains highlighted in red), engage in an edge-to-face stacking interaction that ties together strands of the antiparallel  $\beta$ -sheet in the  $\alpha/\beta$  sandwich fold adopted by KaiB monomeric subunits. The Tyr pairs help stabilize the dimer-dimer interface by forming mostly hydrophobic interactions with E34 and F35 as well as L59 and T63 (side chains highlighted in black; a/d and b/c subunit interfaces). The Y7/93A KaiB double mutant with additional truncations at the N- and C-terminal ends (residues <6 and >93, respectively) exists predominantly in the dimeric form (Chang et al, 2012). The drawing was generated with UCSF Chimera (Pettersen et al, 2004).

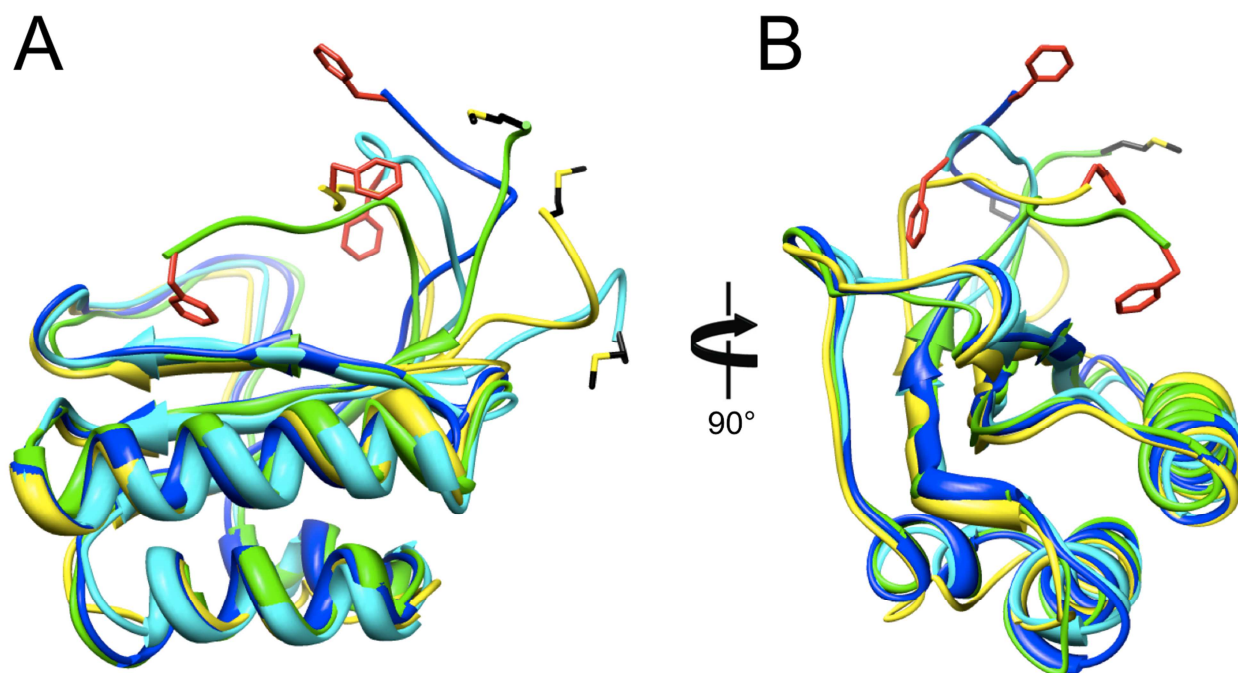


**Figure S4. Flexibility of N- and C-terminal tails in KaiB monomeric subunits.** Superimposition of the a (blue), b (yellow), c (green) and d (cyan) subunits (residues Y8-Y94) viewed **A)** across  $\alpha$ -helices and the  $\beta$ -sheet and **B)** rotated around the vertical by  $90^\circ$ , illustrating the conformational variations in the N- and C-terminal regions. Side chain carbons of N-terminal Met and C-terminal Phe residues are highlighted in black and red, respectively (please note that the first six residues of subunit “a” were not visible in the electron density). The drawing was generated with UCSF Chimera (Pettersen et al, 2004).

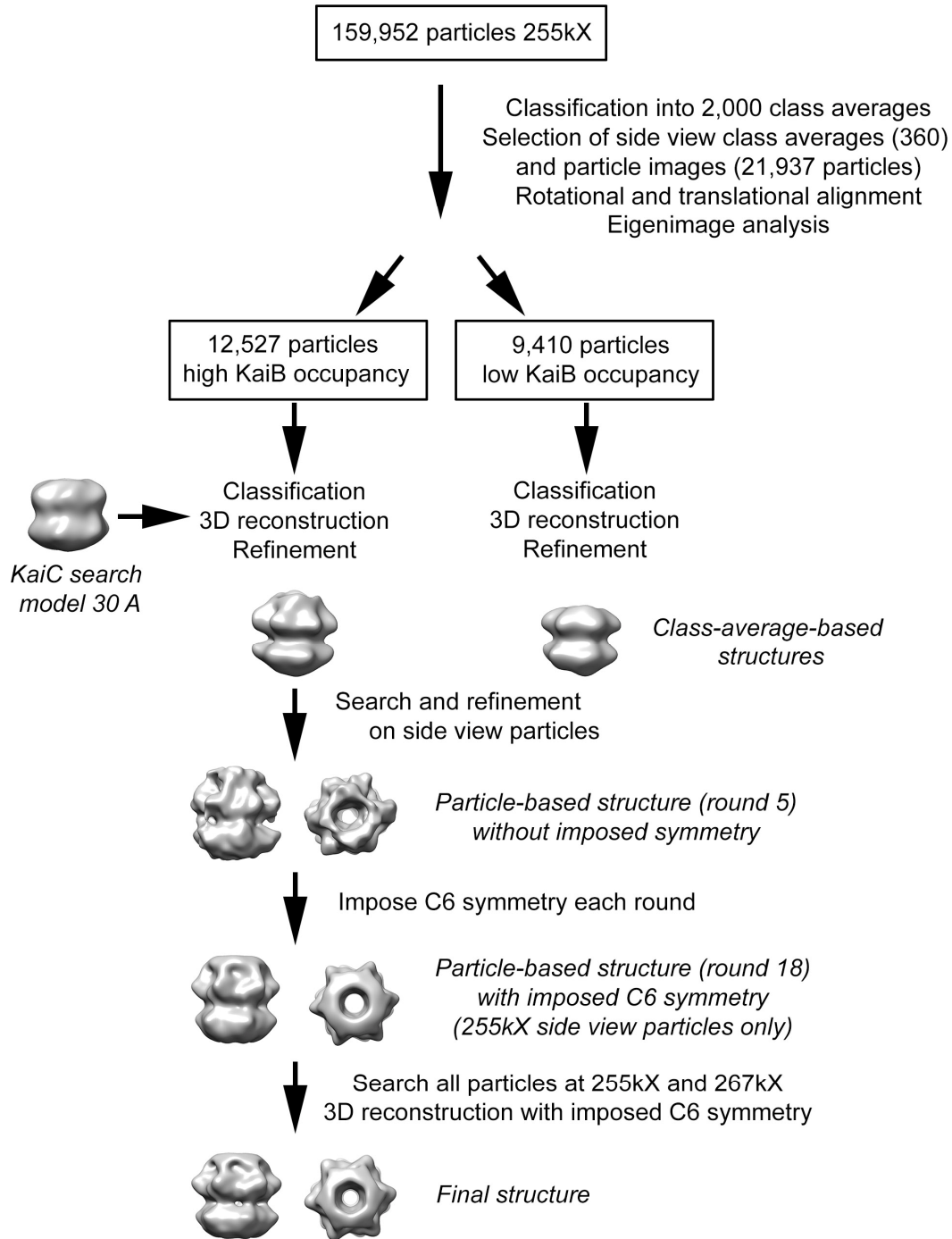


**Figure S5. Schematic outline of the image processing procedure followed to generate the KaiB-KaiC- $\Delta$ 489 cryoEM structure.** The Eigenimage analysis was performed following a procedure applied to GroEL (Clare et al, 2012). See Materials and Methods section for additional details.

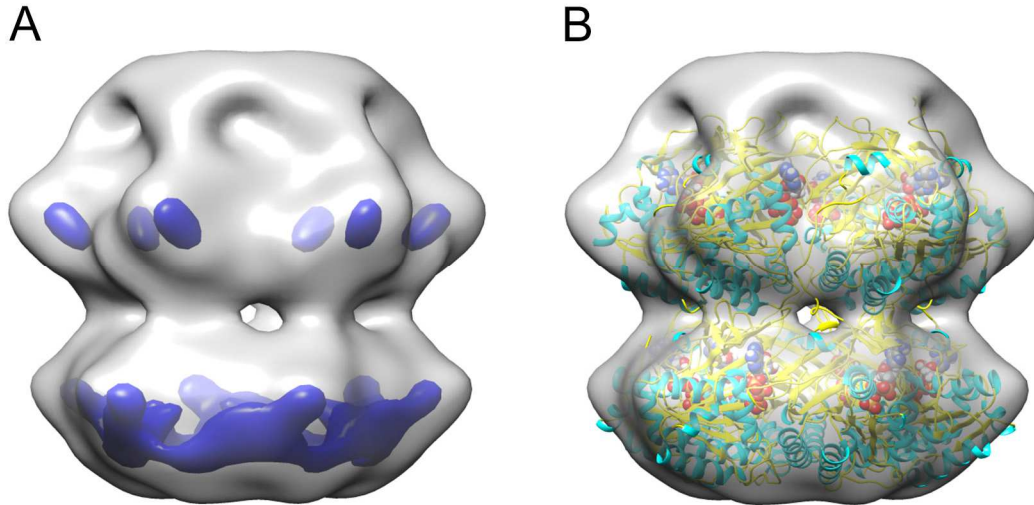


**Figure S6. Strongest density within the KaiB-KaiC- $\Delta$ 489 cryoEM structure aligns with  $\alpha$ -helices in KaiCI. **A)** CryoEM structure displayed with two isosurface levels: contoured for 100% of the expected volume for six KaiB monomers and a KaiC hexamer (transparent gray) and contoured to show just the strongest density (solid blue). **B)** CryoEM structure (transparent gray) with the atomic model for KaiC- $\Delta$ 489 (based on PDB ID 3DVL) after a 100ps MDFF simulation docked with the CII end of KaiC next to KaiB. Alpha-helices are in cyan and ATP molecules are in space filling representation. Note that the strongest density at the base of the KaiB-KaiC- $\Delta$ 489 structure (A) is consistent with  $\alpha$ -helices at the bottom of the CI domain in this KaiC orientation.**

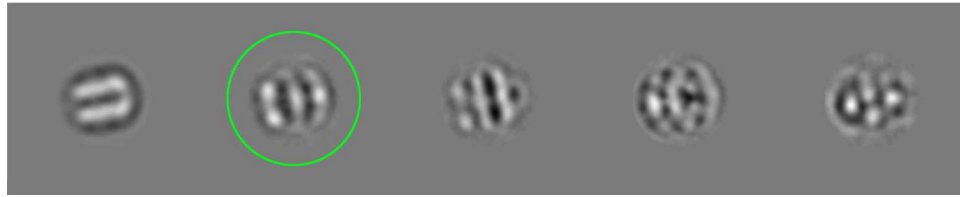


**Figure S7. Eigenimages calculated from the aligned side view particles images.** The first five eigenimages are shown for the dataset collected with a magnification of 255kX. The circled eigenimage was used for sorting the side view particles images into two groups, one with high KaiB occupancy and the other with low KaiB occupancy. This eigenimage predominantly indicates the presence of the KaiB density layer as well as some orientational variation.

**Table S1. Comparison of 16 KaiBC models**

<b>Model</b>	<b>KaiC interaction side</b>	<b>Nonbonded interaction energy between a KaiB monomer and KaiC hexamer (kcal/mol)<sup>a</sup></b>	<b>Buried accessible surface area between a KaiB monomer and KaiC hexamer (Å<sup>2</sup>)</b>
1 <sup>b</sup>	CII	-365	2,143
2	CII	-199	2,055
3	CII	-226	1,968
4	CII	-90	1,653
5	CII	-161	1,626
6	CII	-87	1,697
7	CII	-116	1,841
8	CII	-74	1,613
9	CI	-367	1,331
10	CI	-227	1,170
11	CI	-343	1,418
12	CI	-121	1,110
13	CI	-305	1,219
14	CI	-143	982
15	CI	-174	1,029
16	CI	-49	1,170

- a. Note that negative values for nonbonded interaction energies are favorable  
b. Selected KaiBC model

**Table S2. Robustness of KaiBC interface after molecular dynamics flexible fitting runs with different starting KaiB orientations.** The top ten interaction residues at the end of the MDFF simulation are listed in order of their contribution to the total nonbonded interaction energy between KaiB and KaiC (highest contribution on the left). Interaction residues in common between model 1 and the models with KaiB rotated +/- 10° are highlighted in yellow. For the KaiC interaction residues, the chain is indicated after the residue number.

A. KaiB interaction residues

Model 1	R82	R22	K25	E34	R74	N29	N19	K84	T17	I30
KaiB rotated +10°	R22	K66	R82	E32	E34	E83	K25	N29	R74	I30
KaiB rotated -10°	R22	R74	R82	K84	K25	E34	N29	T26	D45	N19

B. KaiC interaction residues

Model 1	K475.A	D464.A	E272.A	E444.F	E448.F	R269.A	R446.F	S473.A	E448.A	M471.A
KaiB rotated +10°	K475.A	R269.A	E448.F	R468.A	E272.A	E444.F	E448.A	D464.A	E272.B	E469.A
KaiB rotated -10°	E448.F	R269.A	D464.A	E444.F	K475.A	E469.A	R446.F	E272.A	E448.A	V268.A

## SI References

Chang YG, Tseng R, Kuo NW, LiWang A (2012) Rhythmic ring-ring stacking drives the circadian oscillator clockwise. *Proceedings of the National Academy of Sciences of the United States of America* **109**: 16847-16851

Clare DK, Vasishtan D, Stagg S, Quispe J, Farr GW, Topf M, Horwich AL, Saibil HR (2012) ATP-triggered conformational changes delineate substrate-binding and -folding mechanics of the GroEL chaperonin. *Cell* **149**: 113-123

Combet C, Blanchet C, Geourjon C, Deleage G (2000) NPS@: network protein sequence analysis. *Trends in biochemical sciences* **25**: 147-150

Corpet F (1998) Multiple sequence alignment with hierarchical clustering. *Nucleic Acids Research* **16**: 10881-10890

Pettersen EF, Goddard TD, Huang CC, Couch GS, Greenblatt DM, Meng EC, Ferrin TE (2004) UCSF Chimera--a visualization system for exploratory research and analysis. *Journal of Computational Chemistry* **25**: 1605-1612